Efficient, Stable Infrared Photovoltaics Based on Solution-Cast Colloidal Quantum Dots

Ghada I. Koleilat, Larissa Levina, Harnik Shukla, Stefan H. Myrskog, Sean Hinds, Andras G. Pattantyus-Abraham, and Edward H. Sargent*

Department of Electrical and Computer Engineering, University of Toronto, 10 King's College Road, Toronto, Ontario M5S 3G4, Canada

ARTICLE

ABSTRACT Half of the sun's power lies in the infrared. As a result, the optimal bandgaps for solar cells in both the single-junction and even the tandem architectures lie beyond 850 nm. However, progress in low-cost, large-area, physically flexible solar cells has instead been made in organic and polymer materials possessing absorption onsets in the visible. Recent advances have been achieved in solution-cast infrared photovoltaics through the use of colloidal quantum dots. Here we report stable solution-processed photovoltaic devices having 3.6% power conversion efficiency in the infrared. The use of a strongly bound bidentate linker, benzenedithiol, ensures device stability over weeks. The devices reach external quantum efficiencies of 46% in the infrared and 70% across the visible. We investigate in detail the physical mechanisms underlying the operation of this class of device. In contrast with drift-dominated behavior in recent reports of PbS quantum dot photovoltaics, we find that diffusion of electrons and holes over hundreds of nanometers through our PbSe colloidal quantum dot solid is chiefly responsible for the high external quantum efficiencies obtained in this new class of devices.

KEYWORDS: infrared photovoltaics · PbSe nanocrystals · benzenedithiol linker · rectifying junction · carrier transport

Solution-processed photovoltaics offer solar energy harvesting characterized by low cost, ease of processing, physical flexibility, and large area coverage.[1,2] Conjugated polymers,[3] inorganic nanocrystals (NCs),[4] and hybrid materials[5] have been widely investigated and optimized to this purpose. Organic solar cells have already achieved 6.5% solar conversion efficiencies.[6] However, these devices fail to harvest most of the infrared (IR) spectral region. High efficiency multijunction solar cells offer the prospect of exceeding 40% efficiency[7] through the inclusion of infrared-bandgap materials. In this context, infrared single-junction solar cells should be optimized for infrared power conversion efficiency rather than solar power conversion efficiency. For double- and triple-junction solar cells, the smallest-bandgap junction optimally lies at 1320 and 1750 nm, respectively. Attempts to extend organic solar cell efficiency into the near-infrared have so far pushed the absorption onset only to 1000 nm.[8]

By virtue of their size-tunable optical properties, lead salt colloidal quantum dots (CQDs) can be engineered to access the visible and the short-wavelength infrared spectral regions.[9] Recently, organic polymers sensitized using infrared lead salt nanocrystals have been investigated; however, these devices did not exceed monochromatic power conversion efficiencies of 0.1%.[10–14] In 2007, Klem et al. reported 1.3% monochromatic infrared power conversion efficiencies through the use of thiols and high-temperature processes to achieve smooth films on rough nanoporous transparent metal oxides.[15] More recently, the highest infrared monochromatic external quantum efficiency (EQE) yet achieved with nanocrystals was reported: 37% under 12 mW cm^{-2} illumination at 975 nm.[16] These PbS CQD based devices registered an infrared power conversion efficiency of 4.2%.

Herein we report a PbSe CQD based photovoltaic device that achieves 3.6% infrared power conversion efficiency (PCE). This is the first PbSe colloidal quantum photovoltaic to exceed 1% infrared PCE.[13,14] It also represents the first solution-processed infrared photovoltaic device to be stable over weeks without requiring fresh deposition of its top electrical contact.

To achieve this record combination of efficiency and stability, we developed and pursued a materials processing strategy as follows:

- We believed that nanocrystal-capping ligands such as butylamine, although short in length and thus consistent with reasonable carrier transport, are sufficiently labile as to imperil the stable passivation of thin solid films over days and weeks. We therefore selected a more strongly binding end functional group

*Address correspondence to ted.sargent@utoronto.ca.

Received for review February 13, 2008 and accepted April 13, 2008.

Published online May 2, 2008.
10.1021/nn800093v CCC: $40.75

to passivate our nanoparticle surfaces robustly in the solid state.

- We believed that further increase in proximity among the nanoparticles could be achieved and could result in improved electron and hole transport, without sacrificing the highly desired quantum size effect tuning offered by the use of colloidal quantum dots. We therefore pursued a short bidentate linker having a conjugated, instead of entirely insulating, moiety lying between the end groups.[17]
- Finally, we were concerned that too large a change in film volume resulting from the exchange of longer oleic-acid-capped ligands to short cross-linkers would lead to poor film morphology and electrical shorts. We pursued therefore solution-exchange to a shorter linker prior to film formation and film cross-linking.

These considerations, taken together, led us to first use a solution-phase exchange to an intermediate ligand, octylamine, followed by solution-casting of films and finished with a treatment using the bidentate linker, benzenedithiol.

We synthesized PbSe NCs using a modified version of the organometallic route previously reported for PbS NCs.[18] The as-synthesized NCs (Figure 1a) were capped with ~2 nm oleate ligands, previously reported to impede efficient charge transport in films.[12,19] We preceded the benzenedithiol cross-linking (Figure 1c) with a solution-phase ligand exchange (Figure 1b). As a result, the oleate ligands were replaced with shorter octylamine ligands (~1 nm). In this work, we used PbSe NCs having an absorption peak ranging between 1200 and 1300 nm as shown in Figure 1d. We spin-coated thin NC films (~110 nm) on ITO substrates and immersed the samples in a dilute solution of benzenedithiol in acetonitrile (3.5 mM) for a duration ranging from 10 to 30 min. This rendered the layer insoluble in the nonpolar solvents that were used for spin-coating the NCs. We deposited a second thin layer on top to ensure the formation of a smooth, densely packed film. The second layer was also subjected to a linking treatment. The total thickness of the NCs active layer ranged between 210 and 250 nm.

RESULTS

Photovoltaic Device Performance. Figure 2a shows our best recorded infrared power conversion efficiency of 3.6%. The EQE reached 46% under 12 mW cm^{-2} illumination at 975 nm. The devices exhibited a power conversion efficiency of 1.1% under simulated solar illumination at 100 mW cm^{-2} as shown in Figure 2b. The cross-linking process performed on these CQD films was optimized by varying the treatment durations (see Supporting Information S1).

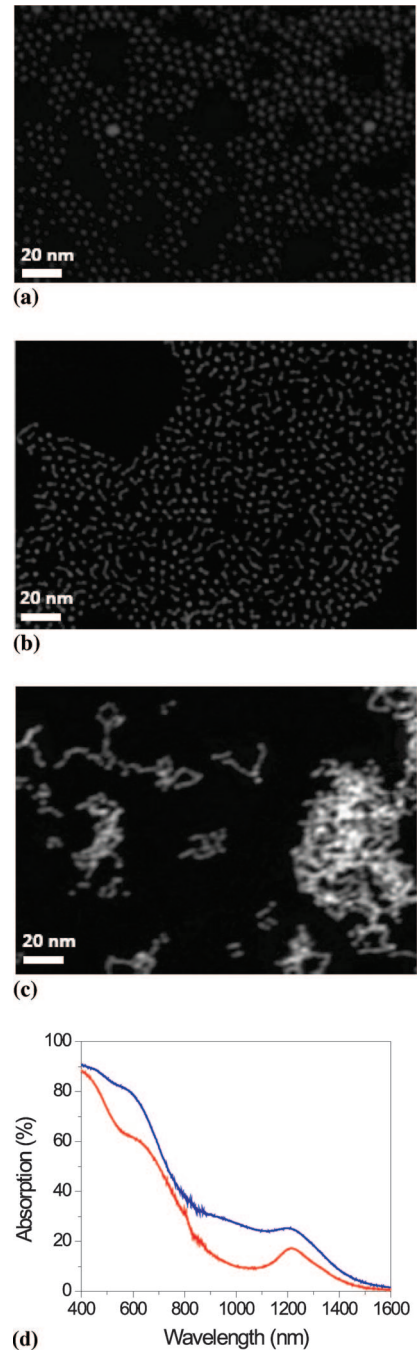

Figure 1. Transmission electron microscopy of PbSe NCs: (a) as-synthesized oleic-acid-capped PbSe NCs used in this investigation (~5 nm in diameter), (b) reduced internanoparticle distance after octylamine ligand exchange, (c) networks of PbSe NCs after benzenedithiol treatment due to the strong affinity of the thiol-end groups for the Pb atoms. (d) Absorption of single treated (red) and double treated (blue) layers.

We present the spectrally resolved EQE between 400 and 1600 nm in Figure 2c. The EQE follows closely the features of the absorption spectrum shown in Figure 1d; a well-defined first excitonic peak is observable at 1250 nm. In the visible wavelengths, a peak EQE of 70% is recorded. From measurements of total film absorbance, we estimated the internal quantum efficiency

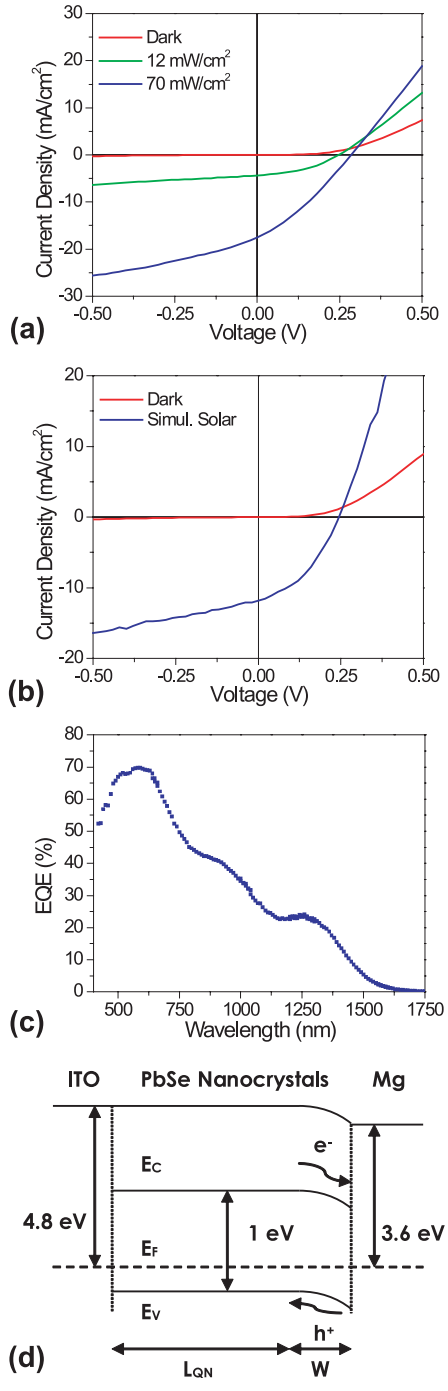

Figure 2. Photovoltaic device performance. Current−voltage characteristics of a benzenedithiol-treated two-layered device exhibiting (a) 3.6% monochromatic power conversion efficiency at 975 nm under 12 mW cm^{-2} illumination, and (b) simulated solar power conversion efficiency of more than 1.1% (*i.e.*, AM1.5 at 100 mW cm^{-2}). (c) Spectral external quantum efficiency of a device reaching 37% in the infrared and about 70% in the visible range. From total absorbance measurements at 975 nm, the IQE was found to approach 90%. (d) Spatial band diagram showing the device model. A Schottky barrier is formed at the Mg/p-type semiconducting NCs interface. The majority of the photogenerated carriers diffuse through the quasi-neutral region (L_{QN}, ~145 nm) and are separated in the depletion region (W, ~65 nm). A fraction of the carriers is lost to recombination.

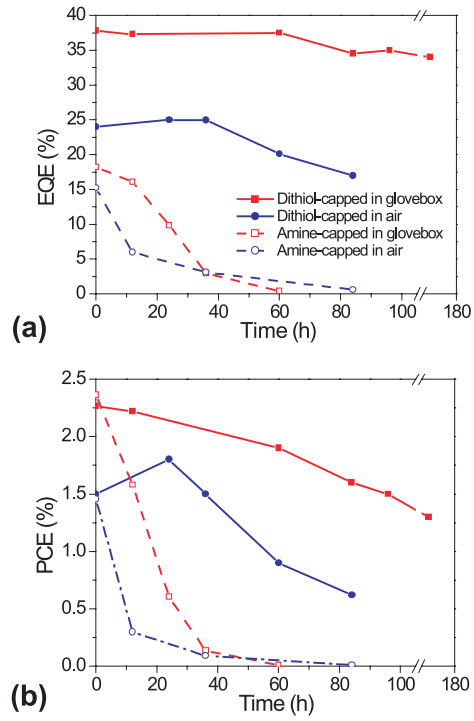

Figure 3. EQE (a) and PCE (b) stability comparison of benzenedithiol-treated PbSe devices with previously reported amine-capped devices stored in air and in inert atmosphere.[16] The benzenedithiol-treated devices retained their high EQE values for over 1 week stored in a nitrogen-filled glovebox (solid red line), and their PCE maintains 90% of its initial value for more than 2 days. The amine-capped devices (dashed red line) severely deteriorated within the first 24 h. In air, the benzenedithiol-treated devices (solid blue lines) registered greater stability than the amine-capped devices (dashed blue lines). Note that all testing was done in air and all devices in this study were exposed to a minimum of 15 h of oxygen and moisture. Several high efficiency benzenedithiol-treated devices retained over 75% of their EQE for more than 2 weeks. The reported EQE and PCE values were taken under 12 mW cm^{-2} at 975 nm.

at 975 nm to approach 90% in the best devices, which implies highly efficient charge separation and extraction.

Our materials processing led to reproducibly high performance: throughout the course of this study, approximately 40 devices were made that exhibited infrared monochromatic power conversion efficiencies in excess of 3%.

Device Stability. Our stability study for devices stored both in air and in nitrogen is summarized in Figure 3. When stored in a nitrogen-filled glovebox for over 2 weeks, devices retained more than 75% of their initial high EQEs. We compared the stability of the devices fabricated in the present work with previously reported high-efficiency devices,[16] fabricated as described by spin-coating butylamine-capped PbS NCs on ITO substrates and evaporating Al contacts on top.[16] The benzenedithiol-cross-linked PbSe NC devices retained their high EQEs over 10 days when stored under nitrogen, whereas the amine-capped devices lost half of

their EQE and more than 75% of their power conversion efficiency within 24 h.

We also compared performance of devices stored in air. The dithiol-capped PbSe NC based devices retained their high EQE and ~80% of their PCE over 48 h, whereas the amine-capped devices lost all performance within the same period of time.

Model of Physical Mechanisms and Origins of High Efficiency. We sought to investigate in greater detail the physical mechanisms responsible for the performance of our best devices and to understand further the process steps that were most critical to the performance improvements reported herein.

We began with an exploration of which of the metal−semiconductor junctions is responsible for providing rectification and charge separation. We then estimated from capacitance−voltage measurements the spatial extent of the resultant depletion region. From this we were able to propose a spatial band diagram.

We then quantified the absorbance of photons in each of the key regions, the depletion and quasi-neutral portions, of the colloidal quantum dot active region. Combining this with knowledge of the depth of the depletion region, the thickness of the device, and the measured EQE, we were able to estimate the minority carrier diffusion length that is required to explain our high overall efficiency.

We then proceeded to investigate whether the electronic properties of our materials are indeed capable of supporting such a long minority carrier diffusion length. We measured electron mobility using the time-of-flight (TOF) method[20] and estimated the carrier lifetime using the open-circuit-voltage decay method.[21] We estimated in this way an electron diffusion length in the range 200−300 nm and found this to be sufficient to account for our high observed efficiencies. We also concluded that further improvement in performance could be achieved by increases in electron mobility leading to even more efficient diffusion from the quasi-neutral region to the edge of the depletion region.

Rectifying Junction and Location of Depletion Region. We turned first to our investigations of the location of the rectifying metal−semiconductor junction, and thus the depletion region, in our devices. We studied this by varying the choice of metal both as bottom and top contact. First, while maintaining ITO as the bottom contact, we deposited Al (~4.2 eV), Ag (~4.3 eV), or Mg (~3.6 eV) atop the NC films. In all cases we obtained similar I−V characteristics, though the open circuit voltages ($V_{oc\_Mg} > V_{oc\_Al} > V_{oc\_Ag}$) were smaller when Ag and Al were used. On the other hand, when we employed Au as top contact, the device exhibits a linear I−V (Supporting Information S2). From this we concluded that the Mg−NC junction is responsible for rectification in our devices.

TABLE 1. Summarizing the Contribution of the Depletion and Quasi-neutral Regions to EQE under 12 mW cm^{-2} Intensity at 975 nm

region	relevant thickness (nm)	absorption (%)	IQE (%)	% contributed to overall EQE
depletion	65	13	>90	>12
quasi-neutral	145	30	65	20
total measured EQE (%): 32				

We also varied the bottom contact, replacing ITO (~4.8 eV) with Pt (~6.3 eV) or Au (~5 eV). All devices continued to provide good rectification when a Mg top contact was employed, and the current−voltage characteristics did not appreciably change. From this we concluded that the bottom contact (transparent ITO in our best devices) serves mainly for ohmic hole collection in our solar cells. On the basis of these conclusions, we propose the spatial band diagram of Figure 2d.

We sought then to determine the depth of the depletion region associated with the Mg−NC junction. We measured the capacitance at zero bias (under short-circuit conditions). We found the static relative permittivity via the charge extraction by the linearly increasing voltage (CELIV) method[22] to be 15 ± 1 (see Supporting Information S6). This allowed us to estimate the depletion width to be 65 ± 5 nm (see Supporting Information S8).

We note as well that, in our experience, all attempts to fabricate CQD devices using PbSe nanocrystals *without* any thiol-based cross-linker[16] failed to produce a photovoltaic effect (see Supporting Information S3). This is in contrast with recent findings with record-setting PbS CQD devices.[16] We tentatively conclude that PbSe NCs are particularly sensitive to the requirement of effective surface passivation.

Photons Absorbed. Having elucidated a simple spatial band diagram, we sought to determine where electron−hole pairs were generated and in which quantities within the two regions of interest, the depletion region, with its charge-separating field, and the quasi-neutral region, in which minority carrier diffusion would serve as the dominant transport mechanism.

We first looked at whether absorption within the depletion region could, on its own, account for our high observed EQEs. From our knowledge of the absorption per unit length of 975 nm light, we summarize in Table 1 the fraction of incident power absorbed in each region. We conclude from this that less than half of the observed short-circuit current is attributable to electron−hole pair generation from absorption within the depletion region (see Supporting Information S4).

To account for the EQE observed, we estimate that two-thirds of the electron−hole pairs photogenerated within the quasi-neutral portion of the device must have diffused to the depletion region to be efficiently

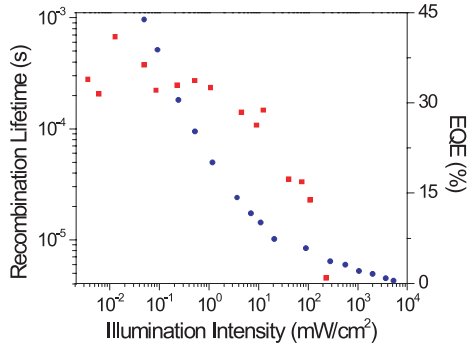

Figure 4. Carrier recombination lifetime (blue, left axis) and external quantum efficiency (red, right axis) versus illumination intensity at 975 nm. The decrease in the EQE (>10 mW cm^{-2}) corresponds to the limit where the minority carrier transit time exceeds the recombination lifetime.

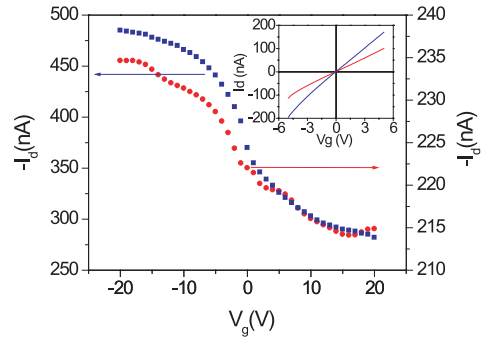

Figure 5. Transfer characteristics of PbSe NC thin-film field-effect transistors. The PbSe NC films exhibit p-type behavior before (red) and after benzenedithiol treatment (blue). I_d-V_d characteristics for both films are shown in the inset. The conductivity, which can be induced from the slope of the I_d-V_d curves, increased after treatment.

separated therein and extracted therefrom. Such a result would be possible only if the minority carrier diffusion length for electrons in the quasi-neutral region were to exceed a few hundred nanometers.

Hole and Electron Mobilities and Lifetimes. To evaluate the feasibility of the electron and hole drift over the depletion region depth (~65 nm) and the electron minority carrier diffusion over the quasi-neutral region depth (~145 nm), we next turned to measuring electron and hole mobilities. When combined with carrier lifetimes, these enable the drift and diffusion lengths to be estimated.

We studied minority electron carrier mobility using the TOF method[20] and the majority carrier mobility via charge extraction by CELIV.[22]

TOF experiments employed a sample with a geometry identical to that of the photovoltaic device, *i.e.*, a layer of NCs sandwiched between the ITO and magnesium contacts, with the exception that the total NC layer in this case was thicker (>500 nm). We found the electron mobility to be 1.4×10^{-3} cm^2 V^{-1} s^{-1} for a benzenedithiol-treated device (see Supporting Information S5). CELIV experiments conducted on the photovoltaic devices allowed us to estimate the hole mobility to be 2.4×10^{-3} cm^2 V^{-1} s^{-1} in the dithiol treated NC based devices (see Supporting Information S6). Thus, the electron and the hole mobilities in our devices are within the same order of magnitude, in contrast with recent findings in PbS colloidal quantum dots devices,[16] where the minority electrons were ~8 times less mobile.

We then sought to estimate the recombination lifetime τ at relevant solar intensities through the technique of transient open circuit voltage decay (OCVD).[21] We illuminated the device using a digitally modulated 975 nm diode laser at different intensities (Figure 4). At 12 mW cm^{-2} we found the lifetime to be on the order of 10−20 μs (see Supporting Information S7).

We fabricated thin-film field-effect transistors (FET) on highly conductive silicon wafers with 100 nm of thermally grown oxide as the gate dielectric. The source and drain electrodes were separated by a 10 μm gap. In order to spin-coat films 50 nm thick, we diluted the octylamine-capped PbSe NCs to a concentration of 10 mg mL^{-1} and the benzenedithiol solution to 1 mM. For constant drain source voltage, we applied a range of gate voltages and recorded the current modulation through the NC film.

Figure 5 shows the FET transfer characteristics of NC films directly deposited from solution and after exposure to benzenedithiol treatment. In both cases, the drain current (I_d) increases in magnitude as the applied gate voltage (V_{gs}) becomes more negative. This suggests the formation of a p-channel in the FET devices indicative of the p-type behavior[23] of the PbSe NCs (see Supporting Information S9).

Drift and Diffusion Lengths. Carriers in the depletion region are separated via the action of the built-in field resultant from the metal-semiconductor, or Schottky, junction. The drift length is given by $(\mu\tau V_{bi})/W$, where μ is the carrier mobility, V_{bi} is the built-in potential, and W is the depletion width. Under short-circuit conditions at 12 mW cm^{-2} and assuming a built-in voltage of 0.3 V,[24,25] we estimated drift lengths of 8.5 μm for electrons and 14.5 μm for holes. In sum, we expect no difficulty in removing each carrier type from the 65 nm thick depletion region.

In the quasi-neutral region, charge transport occurs mainly through diffusion and the carrier diffusion length may be obtained from $\sqrt{[\mu\tau((kT)/q)]}$. The calculated electron minority diffusion length is in excess of 220 nm, which allows a substantial fraction of the minority carriers to diffuse out of the neutral region, and allows us to account for the high observed EQE (see Supporting Information S10). Table 2 summarizes the calculated charge transport characteristics.

Carrier extraction in these photovoltaic devices, as a result of the narrow depletion region, is critically dependent on diffusion enabled by high minority carrier mobility and long lifetime. This contrasts with recent

TABLE 2. Summary of Charge Transport Parameters for Photovoltaic Devices Based on Benzenedithiol-Treated PbSe NCs at the Operating Intensity of 12 mW cm^{-2} at 975 nm and under Low Injection Regime

carriers	mobility (cm^2/Vs)	recombination lifetime (μs)	drift length (μm)	diffusion length (nm)
electrons	1.4×10^{-3}	>13	8.5	220
holes	2.4×10^{-3}	>13	14.5	285

findings in drift-dominated PbS Schottky-barrier devices.[24]

We further corroborated our proposed physical picture by investigating the dependence of EQE and recombination as a function of illumination intensity, as seen in Figure 4. The EQE began to diminish at intensities greater than 10 mW cm^{-2}. From OCVD measurements, the recombination lifetime drops below about 10 μs at such intensities. In view of the electron mobility, the electron diffusion length begins to contract well below the quasi-neutral region thickness under such conditions, accounting for the onset of EQE roll-off.

DISCUSSION

With this performance and physical picture explained, we now discuss the role of our chosen bidentate linker. The first expected impact of linking nanoparticles in the solid state is to bring the particles closer together (Figure 1a−c). Figure 1c shows that benzendithiol molecules are most likely cross-linking the PbSe nanoparticles. Specifically, both electron and hole mobilities increased by more than 1 order of magnitude as a result of cross-linking (see Supporting Information S5). Even with the mobility-increasing treatments, the films retained their quantum size effect, as seen in absorption spectra and external quantum efficiency spectra.

We noted above that diffusion plays a much larger role in our devices than in the best reported PbS solar cells. The electron mobility of our devices is seven times greater than in the PbS CQD report,[24] a fact that accounts for a doubling of the electron minority diffusion length in our materials system. Benzenedithiol is in fact a molecular conductor in view of its delocalization of electron molecular orbitals.[17] In addition, conjugated dithiol molecules used to bridge quantum dot systems have previously been reported not only to link nanocrystals but also to provide a pathway for electron transfer.[26]

The devices reported herein exhibited a photovoltaic response only after being subjected to the benzenedithiol cross-linking process. We propose that the as-exchanged NCs were dominated by a large density of unpassivated surface states. As with previously reported chemical processes on PbSe and CdSe NCs,[27−33] benzenedithiol offers passivation of dangling bonds. Additionally, as seen in our stability study, benzenedithiol appears to offer a longer-lived NC−metal interface than amine ligands. The latter are believed to react with the top metal contact.

Another feature of the device processing architecture employed herein is the use of two superimposed layers of colloidal quantum dot solids. Our purpose was to increase absorbing thickness and minimize pinholes. Preceding the solid-state treatment with a solution-phase exchange to a somewhat shorter ligand helped to reduce volume contraction upon cross-linking of the film. This contributed to the realization of densely packed, high-mobility films *in situ* on a substrate.

In sum, the present work demonstrates a stable, high-efficiency infrared solution-processed photovoltaic device. Remarkably, the work shows that minority carrier diffusion can occur efficiently over hundreds of nanometers in such films. Strongly passivating, short, electron-transport-assisting bidentate linkers appear to play a key role in achieving these properties.

MATERIALS AND METHODS

Chemicals. Lead(II) oxide powder (PbO, 99%), oleic acid (OA, technical grade 90%), 1-octadecene (ODE, technical grade 90%), anhydrous toluene, octane, methanol, isopropanol, acetonitrile, and ethyl acetate were purchased from Sigma-Aldrich. Bis(trimethylsilyl)selenide (TMSe, >97% purity) was purchased from Gelest, Inc. 1,4-Benzenedithiol (97%) was purchased from Alpha Aesar.

PbSe Synthesis and Ligand-Exchange Procedure. ODE was degassed by prepumping at 80 °C for 16 h, and the TMSe source was prefiltered with 0.1 and 0.02 μm Whatman syringe filters before use. The synthesis was performed in a single, three-neck, round-bottom flask. The Pb precursor was prepared by pumping the mixture of PbO and OA at 80 °C for 16 h. The resulting transparent solution of lead oleate precursor was stirred vigorously while being heated under Ar for about 30 min. The stock solution of selenium precursor was prepared by mixing TMSe with ODE in a glovebox and the portion corresponding to a 2:1 (Pb/Se) molar ratio was rapidly injected into the reaction flask. The injection temperature ranged between 125 °C for smaller nanocrystals and 140 °C for the largest NCs. Upon injection, nucleation occurs instantly; thus, rapid injection is critical to achieve a narrow size distribution. After injection, the temperature of the reaction was dropped, and the reaction was quenched by subjecting it to a water−ice bath for 1 min and 40 s. A typical synthesis for NCs having their excitonic peak ranging from 1200 to 1300 nm involved injecting of 7 mL of selenium stock solution (1 mmol of TMSe) into the reaction flask containing 2 mmol of PbO (0.45 g) and 63 mmol of OA. PbSe NCs, particularly in their solution phase, were observed to be extremely sensitive to both air and moisture, and as a result all postsynthetic treatments were performed in a glovebox with anhydrous reagents. The oleate-capped PbSe NCs were isolated from any remaining starting materials and side products by precipitating the solution with a mixture of equal volumes of methanol (5 mL) and ethylacetate (5 mL). The precipitate was then redispersed in toluene and reprecipitated with methanol. After the second precipitation, the NCs were vacuum-dried for 10 min and redispersed in toluene.

The solution exchange procedure was carried out inside a nitrogen-filled glovebox. The as-synthesized NCs were precipi-

tated with methanol, vacuum-dried for 10 min, and redispersed in octylamine. After 3 days, we precipitated the NCs with anhydrous isopropanol, vacuum-dried them for 10 min, and redispersed them in octane solution to achieve a typical concentration of 80 mg mL^{-1}.

Device Fabrication, Testing, and Characterization. The octylamine-exchanged PbSe NCs were spin-coated on ITO-coated glass substrate inside the glovebox. The devices had a typical thickness of 210−250 nm as measured with a surface profiler (Veeco Dektak3). The benzenedithiol treatment was done in a fumehood in air. We deposited 100 nm Mg/190 nm Ag by thermal evaporation through a shadow mask, leading to a contact area of 3.1 mm^2. We stored the devices in a nitrogen-filled glovebox for 24 h before initial testing. All device characterizations were carried out in dark shielded enclosures in air.

All current−voltage measurements including FET characterizations were taken with an Agilent 4155C semiconductor parameter analyzer. For the IR characterizations, the devices were illuminated through the ITO-coated glass using a continuous-wave diode laser operating at 975 nm. An Oriel solar simulator operating at 100 mW cm^{-2} was used to simulate the solar spectrum under AM1.5 conditions. The illumination intensity was measured with a Melles-Griot broadband power meter.

For the TOF measurements, thick samples (>600 nm) were excited using a yttrium-aluminum-garnet (YAG) laser operating at 532 nm with 10 ns pulses at a 10 Hz repetition rate. The light was incident on the sample from the transparent ITO side. The devices were biased using a Keithley 2400 Source Meter, and a digital oscilloscope was used to measure the current transient output across a 50 Ω load. The CELIV measurements were carried out using an Agilent 33120A function generator that provided the linearly increasing voltage signals, and the current output was measured across a 50 Ω load with a Tektronix TDS 220 digital oscilloscope.

The OCVD transients were recorded using a digital oscilloscope with a 1 MΩ input impedance. The illumination source (975 nm diode laser) was modulated using a Stanford Research Systems DG535 digital pulse generator. An Agilent 4284A LCR meter was used to measure the capacitance at zero bias in order to determine the device depletion width.

For the external quantum efficiency spectrum measurements, the incident light was chopped at 100 Hz and the short-circuit current was measured with a Stanford Research SR830 lock-in amplifier. Illumination was provided by a white light source dispersed by a Jobin-Yvon Triax 320 monochromator. The light intensity was kept constant for all wavelengths. The measured spectrum was then scaled to match the value of the monochromatic EQE obtained at 975 nm.

We obtained the total film absorbance by measuring the reflectivity of the substrate and correcting for the ITO and Mg contact absorption in an integrating sphere. A Cary 500 UV−vis−IR Scan photospectrometer in the reflective mode was used to measure the reflectivity spectra. TEM images were taken using a Hitachi HD-2000.

Acknowledgment. The authors thank G. Konstantatos, K. Johnston, J. Clifford, E. Klem, L. Soleymani, and J. Tang for many helpful discussions. Funding for this research was provided by the Natural Sciences and Engineering Research Council (NSERC) of Canada under its Strategic Grants program.

Supporting Information Available: Optimization of benzenedithiol treatment, current−voltage characteristics of different top metal contacts, current−voltage characteristics of devices with no postfabrication treatment, and the contribution of the different portions of the active layer to EQE, ToF, CELIV, OCVD, C−V and FET measurements. This material is available free of charge *via* the Internet at http://pubs.acs.org.

REFERENCES AND NOTES

1. Hoppe, H.; Sariciftci, N. S. Organic Solar Cells: An Overview. *J. Mater. Res.* **2004**, *19*, 1924–1945.
2. Sargent, E. H. Infrared Quantum Dots. *Adv. Mater.* **2005**, *17*, 515–522.
3. Kim, K.; Liu, J.; Namboothiry, M. A. G.; Carroll, D. L. Roles of Donor and Acceptor Nanodomains in 6% Efficient Thermally Annealed Polymer Photovoltaics. *Appl. Phys. Lett.* **2007**, *90*, 163511.
4. Gur, I.; Fromer, N. A.; Geier, M. L.; Alivisatos, A. P. Air-Stable All-Inorganic Nanocrystal Solar Cells Processed from Solution. *Science* **2005**, *310*, 462–465.
5. Gur, I.; Fromer, N. A.; Chen, C.; Kanaras, A. G.; Alivisatos, A. P. Hybrid Solar Cells with Prescribed Nanoscale Morphologies Based on Hyperbranched Semiconductor Nanocrystals. *Nano Lett.* **2007**, *7*, 409–414.
6. Kim, J. Y.; Lee, K.; Coates, N. E.; Moses, D.; Nguyen, T.; Dante, M.; Heeger, A. J. Efficient Tandem Polymer Solar Cells Fabricated by All-Solution Processing. *Science* **2007**, *317*, 222–225.
7. Marti, A.; Araujo, G. L. Limiting Efficiencies for Photovoltaic Energy Conversion in Multigap Systems. *Sol. Energy Mater. Sol. Cells* **1996**, *43*, 203–222.
8. Wienk, M. M.; Turbiez, M. G. R.; Struijk, M. P.; Fonrodona, M.; Janssen, R. A. J. Low-Band Gap Poly(di-2-thienylthienopyrazine):Fullerene Solar Cells. *Appl. Phys. Lett.* **2006**, *88*, 153511.
9. Wise, F. Lead Salt Quantum Dots: The Limit of Strong Quantum Confinement. *Acc. Chem. Res.* **2000**, *33*, 773–780.
10. McDonald, S. A.; Konstantatos, G.; Zhang, S.; Cyr, P. W.; Klem, E. J. D.; Levina, L.; Sargent, E. H. Solution-Processed PbS Quantum Dot Infrared Photodetectors and Photovoltaics. *Nat. Mater.* **2005**, *4*, 1–5.
11. Maria, A.; Cyr, P. W.; Klem, E. J. D.; Levina, L.; Sargent, E. H. Solution-Processed Infrared Photovoltaic Devices with >10% Monochromatic Internal Quantum Efficiency. *Appl. Phys. Lett.* **2005**, *87*, 213112.
12. Zhang, S.; Cyr, P. W.; McDonald, S. A.; Konstantatos, G.; Sargent, E. H. Enhanced Infrared Photovoltaic Efficiency in PbS Nanocrystal/Semiconducting Polymer Composites: 600-Fold Increase in Maximum Power Output via Control of the Ligand Barrier. *Appl. Phys. Lett.* **2005**, *87*, 233101.
13. Cui, D.; Xu, J.; Zhu, T.; Paradee, G.; Ashok, S.; Gerhold, M. Harvest of Near Infrared Light in PbSe Nanocrystal−Polymer Hybrid Photovoltaic Cells. *Appl. Phys. Lett.* **2006**, *88*, 183111.
14. Jiang, X.; Schaller, R. D.; Lee, S. B.; Pietryga, J. M.; Klimov, V. I.; Zakhidov, A. A. PbSe Nanocrystal/Conducting Polymer Solar Cells with an Infrared Response to 2 Microns. *J. Mater. Res.* **2007**, *22*, 2204–2210.
15. Klem, E. J. D.; MacNeil, D. D.; Cyr, P. W.; Levina, L.; Sargent, E. H. Efficient Solution-Processed Infrared Photovoltaic Cells: Planarized All-Inorganic Bulk Heterojunction Devices via Inter-Quantum-Dot Bridging during Growth from Solution. *Appl. Phys. Lett.* **2007**, *90*, 183113.
16. Johnston, K. W.; Pattantyus-Abraham, A. G.; Clifford, J. P.; Myrskog, S. H.; MacNeil, D. D.; Levina, L.; Sargent, E. H. Schottky-Quantum Dot Photovoltaics for Efficient Infrared Power Conversion. Appl. Phys. Lett. 2008, accepted for publication.
17. Dadosh, T.; Gordin, Y.; Krahne, R.; Khivrich, I.; Mahalu, D.; Frydman, V.; Sperling, J.; Yacoby, A.; Bar-Joseph, I. Measurement of the Conductance of Single Conjugated Molecules. *Nature* **2005**, *436*, 677–680.
18. Hines, M. A.; Scholes, G. D. Colloidal PbS Nanocrystals with Size-Tunable Near-Infrared Emission: Observation and Post-synthesis Self-Narrowing of the Particle Size Distribution. *Adv. Mater.* **2003**, *15*, 1844–1849.
19. Konstantatos, G.; Howard, I.; Fischer, A.; Hoogland, S.; Clifford, J.; Klem, E.; Levina, L.; Sargent, E. H. Ultrasensitive Solution-Cast Quantum Dot Photodetectors. *Nature* **2006**, *442*, 180–183.
20. Naka, S.; Okada, H.; Onnagawa, H.; Tsutsui, T. High Electron Mobility in Bathophenanthroline. *Appl. Phys. Lett.* **2000**, *76* (2), 197–199.
21. Mahan, J. E.; Ekstedt, T. W.; Frank, R. I.; Kaplow, R. Measurement of Minority Carrier Lifetime in Solar Cells from Photo-Induced Open-Circuit Voltage Decay. *IEEE Trans. Electron Devices* **1979**, *ED-26*, 733–739.

22. Juska, G.; Arlauskas, K.; Viliunas, M.; Kocka, J. Extraction Current Transients: New Method of Study of Charge Transport in Microcrystalline Silicon. *Phys. Rev. Lett.* **2000**, *84*, 4946–4949.
23. Mentzel, T. S.; Porter, V. J.; Geyer, S.; MacLean, K.; Bawendi, M. G.; Kastner, M. A. Charge Transport in PbSe Nanocrystal Arrays. *Phys. Rev. B* **2008**, *77*, 075316.
24. Johnston, K. W.; Pattantyus-Abraham, A. G.; Clifford, J. P.; Myrskog, S. H.; Hoogland, S.; Shukla, H.; Klem, E. J. D.; Levina, L.; Sargent, E. H. Efficient Schottky-Quantum Dot Photovoltaics: The Roles of Depletion, Drift, and Diffusion. *Appl. Phys. Lett.* **2008**, *92*, 122111.
25. Clifford, J. P.; Johnston, K. W.; Levina, L.; Sargent, E. H. Shottky Barriers to Colloidal Quantum Dot Films. *Appl. Phys. Lett.* **2007**, *91*, 253117.
26. Ouyang, M.; Awschalom, D. Coherent Spin Transfer between Molecularly Bridged Quantum Dots. *Science* **2003**, *301* (5636), 1074–1078.
27. Ginger, D. S.; Greenham, N. C. Charge Injection and Transport in Films of CdSe Nanocrystals. *J. Appl. Phys.* **2000**, *87*, 1361–1368.
28. Yu, C. W.; Guyot-Sionnest, P. N-Type Conducting CdSe Nanocrystal Solids. *Science* **2003**, *300*, 1277–1280.
29. Oertel, D. C.; Bawendi, M. G.; Arango, A. C.; Bulovic, V. Photodetectors Based on Treated CdSe Quantum-Dot Films. *Appl. Phys. Lett.* **2005**, *87*, 213505.
30. Yu, D.; Wehrenberg, B. L.; Jha, P.; Ma, J.; Guyot-Sionnest, P. Electronic Transport of *n*-type CdSe Quantum Dot Films: Effect of Film Treatment. *J. Appl. Phys.* **2006**, *99*, 104315.
31. Talapin, D. V.; Murray, C. B. PbSe Nanocrystal Solids for n- and p-Channel Thin Film Field-Effect Transistors. *Science* **2005**, *310*, 86–89.
32. Murphy, J. E.; Beard, M. C.; Nozik, A. J. Time-Resolved Photoconductivity of PbSe Nanocrystal Arrays. *J. Phys. Chem. B* **2006**, *110*, 25455–25461.
33. Luther, J. M.; Law, M.; Song, Q.; Perkins, C. L.; Beard, M. C.; Nozik, A. J. Structural, Optical, and Electrical Properties of Self-Assembled Films of PbSe Nanocrystals Treated with 1,2-Ethanedithiol. *ACS Nano* **2008**, *2*, 271–280.